Carderock Division
Naval Surface Warfare Center
West Bethesda, Maryland 20817-5700

NSWCCD-50-TR-2009 / 017 March 2009
Hydromechanics Department Report

The Distribution of Breaking and Non-breaking Wave Impact Forces

by

Anne M. Fullerton
Ann Marie Powers
Don C. Walker
Susan Brewton

REPORT DOCUMENTATION PAGE

Form Approved
OMB No. 0704-0188

1. AGENCY USE ONLY (Leave blank)	2. REPORT DATE	3. REPORT TYPE AND DATES COVERED
	March 2009	Final

4. TITLE AND SUBTITLE
The Distribution of Breaking and Non-breaking Wave Impact Forces

5. FUNDING NUMBERS
Contract No.:
N0001408WX20892/AA
Work Unit:
08-1-5600-271

6. AUTHOR(S)
Anne M. Fullerton, Ann Marie Powers, Don C. Walker, Susan Brewton

7. PERFORMING ORGANIZATION NAME(S) AND ADDRESS(ES)
Carderock Division, Naval Surface Warfare Center
Code 5600
9500 MacArthur Boulevard
West Bethesda, Maryland 20817-5700

8. PERFORMING ORGANIZATION REPORT NUMBER
NSWCCD-50-TR-2009 / 017

9. SPONSORING / MONITORING AGENCY NAME(S) AND ADDRESS(ES)
Dr. Ron Joslin
Office of Naval Research
800 North Quincy Street
Arlington, VA 22217-5660

10. SPONSORING / MONITORING AGENCY REPORT NUMBER

11. SUPPLEMENTARY NOTES

12a. DISTRIBUTION / AVAILABILITY STATEMENT
Approved for Public Release; Distribution Unlimited.

12b. DISTRIBUTION CODE

13. ABSTRACT *(Maximum 200 words)*

The magnitude of wave impact loads varies greatly, depending upon whether the wave is breaking, as well as on the wave height, length, steepness, and the geometry and immersion of the impacted structure. This report describes an experiment that was performed to characterize the distribution of breaking and non-breaking wave impact loads over a surface, similar to those performed in 2005 with non-breaking wave impact loads and those performed in 2007 with breaking wave impact loads. In those experiments, the average loads were measured on a flat plate and a cylinder. In order to better understand the distribution of forces over a surface, the impact pressures in this experiment were measured on an instrumented test cube by using an array of slam panels and pressure gages. Plots of impact magnitude trends with wave height, wavelength, draft, and impact angle are presented. Overall, average impact pressures from the breaking waves are greater in magnitude than the impact pressures from the non-breaking waves and average impact pressures tend to increase with increased speed, though there was a dip in pressure at an intermediate speed for some panel locations.

14. SUBJECT TERMS	15. NUMBER OF PAGES
	28+iv
	16. PRICE CODE

17. SECURITY CLASSIFICATION OF REPORT	18. SECURITY CLASSIFICATION OF THIS PAGE	19. SECURITY CLASSIFICATION OF ABSTRACT	20. LIMITATION OF ABSTRACT
Unclassified	Unclassified	Unclassified	Unclassified

This page left intentionally blank.

CONTENTS

FIGURES

TABLES

ABSTRACT

The magnitude of wave impact loads varies greatly, depending upon whether the wave is breaking, as well as on the wave height, length, steepness, and the geometry and immersion of the impacted structure. This report describes an experiment that was performed to characterize the distribution of breaking and non-breaking wave impact loads over a surface, similar to those performed in 2005 with non-breaking wave impact loads and those performed in 2007 with breaking wave impact loads. In those experiments, the average loads were measured on a flat plate and a cylinder. In order to better understand the distribution of forces over a surface, the impact pressures in this experiment were measured on an instrumented test cube by using an array of slam panels and pressure gages. Plots of impact magnitude trends with wave height, wavelength, draft, and impact angle are presented. Overall, average impact pressures from the breaking waves are greater in magnitude than the impact pressures from the non-breaking waves and average impact pressures tend to increase with increased speed, though there was a dip in pressure at an intermediate speed for some panel locations.

ACKNOWLEDGEMENTS

The authors would like to thank Edward Ammeen, David Drazen, David Hess, and Sherece Wade (Code 5600), Thomas Fu (Code 5800), Mark Lundy (Code 653), Mary Lee Pence (Computer Sciences Corporation), and Matthew Weldon (Applied Research Laboratory at Pennsylvania State University) for their valuable assistance on this project.

ADMINISTRATIVE INFORMATION

The work described in this report was performed by the Maneuvering and Control (Code 5600) Division of the Hydromechanics Department at the Naval Surface Warfare Center, Carderock Division (NSWCCD). The work was sponsored by the Office of Naval Research, under the Dynamics of Interaction Platforms Program, Program Manager Dr. Ron Joslin, performed under contract number N0001408WX20892/AA, work unit 08-1-5600-271.

INTRODUCTION

The magnitude of wave impact loads varies greatly, depending upon whether the wave is breaking, as well as on the wave height, length, steepness, and the geometry and immersion of the impacted structure. Chan and Melville (1,2,3,4) have performed several experiments to investigate the force of plunging breakers on flat plates and vertical cylinders. The results of these investigations show breaking wave impact pressures as high as $10\rho c^2$ on plates and cylinders, where ρ is the density of water and c is the wave celerity, which correspond to almost 2000 pounds per square foot for a wavelength of 20 feet. Experimental results from Zhou, Chan and Melville (5) found breaking wave impact

pressures of up to $15\rho e^2$ on a vertical cylinder, which correspond to 3000 pounds per square foot for a wavelength of 20 feet. Field data collected by Bullock and Obhrai (6) shows pressures of over 8000 pounds per square foot on a breakwater for an incident wave height of 10 feet. All of these results suggest that there can be significant variation in the magnitudes of incident wave loads. Additionally, this literature implies that wave impact pressures are dependent on wave characteristics.

This report describes an experiment that was performed to characterize the distribution of breaking and non-breaking wave impact loads over a surface, similar to those performed in 2005 (7,8,9) with non-breaking wave impact loads and those performed in 2007 (10) with breaking wave impact loads. In those experiments, the average loads were measured on a flat plate and a cylinder. In order to better understand the distribution of forces over a surface, the impact pressures in this experiment were measured on an instrumented test cube by using an array of slam panels and pressure gages. The objective of this work is to develop improved understanding of the physics of breaking wave impacts and to investigate the trends of wave slap loads under various wave height, wavelength, impact angle, and draft conditions.

EXPERIMENTAL APPROACH

Wave impact testing was performed in August and September 2008. The instrumented cube was suspended from Carriage 5 and held stationary in the High Speed Tow Basin approximately 200 feet from the wavemaker. The total length of the basin is approximately 1687 feet, and the width of the basin in this section is 21 feet. This basin is equipped with a pneumatic wavemaker dome which is connected to a blower powered by a direct coupled variable speed DC electric motor rated at 100hp, 1150 rpm. A diagram of Carriage 5 is shown in Figure 1 (11).

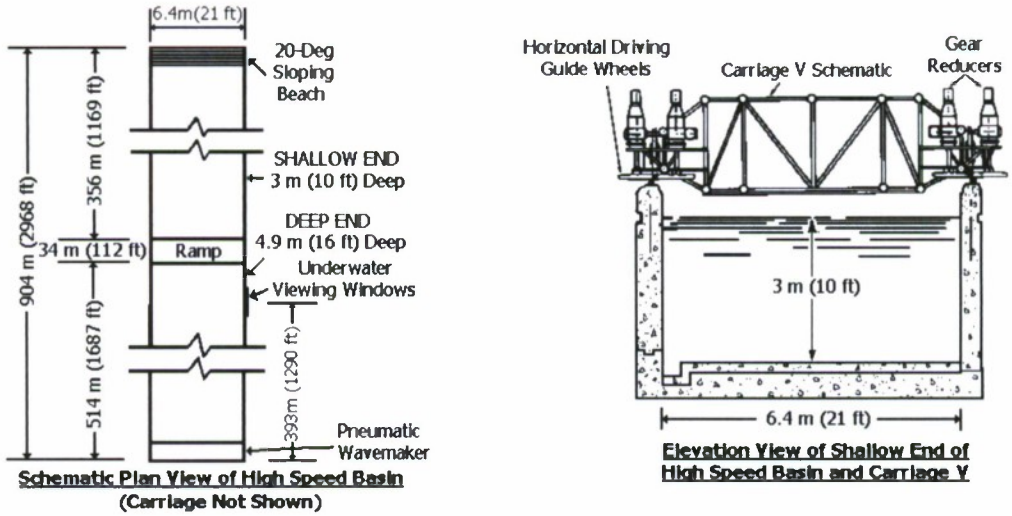

Figure 1: Schematic of high speed tow basin, Carriage 5.

Model Description

The distribution of wave impact loads was measured over the top and front faces of a one cubic foot model constructed of aluminum. The measurement cube was outfitted with a removable instrumented plate which had 9 slam panels of varying sizes and 11 pressure gages (Figure 2). Two side boxes were utilized on either end of the model to limit the wave effects to two dimensions (Figure 3). These boxes were not directly attached to the test cube.

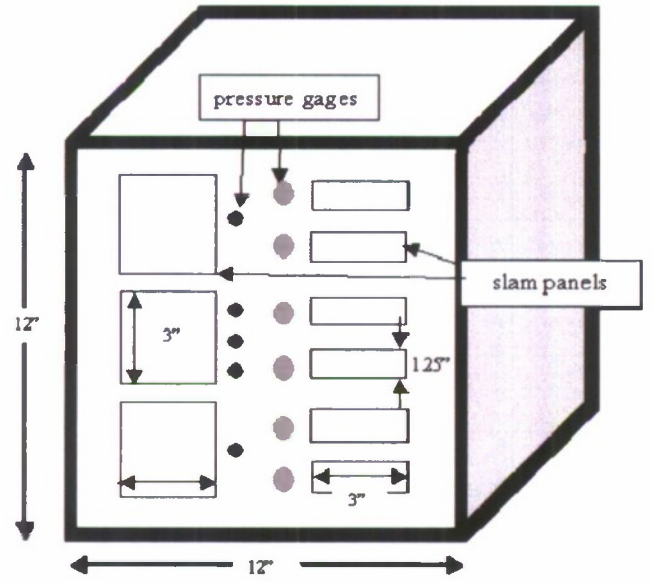

Figure 2. Diagram of test cube with slam panels and pressure gages.

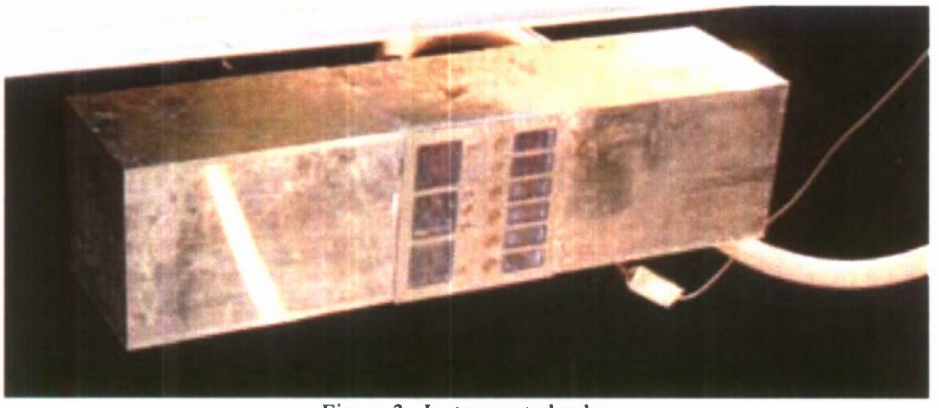

Figure 3. Instrumented cube.

Test Conditions

Table 1 shows the test matrix for this experiment. Three different non-breaking conditions and one breaking wave condition were tested. Tests were run at three different levels of plate submergence (full, half and none), and three different plate angles (0°, +45° toward the incoming wave, -45° away from the incoming wave), as shown in Figure 4. The instrumented plate was used on both the front and top face of the cube. A limited set of runs were made with speed over a range of 0.5 to 2 knots in order to investigate the added forces due to forward motion. Runs were typically made for 3-5 minutes to gather sufficient wave data, which allowed for approximately 75-150 waves to pass (wave periods ranged from 1.97 s to 2.4 s). Each condition was run twice to ensure repeatability.

The breaking waves were generated by sending an external voltage signal made up of 9 waves of varying frequencies (Figure 5), similar to the experiment described in (10). The waves that were generated to create the breaking wave are the larger waves in Figure 5 (greater than 6 volts); the smaller waves are inserted to create a smooth input signal so that the wavemaker did not have to come to an abrupt stop between waves. The input signal waves are listed in Table 2, where the amplitude is shown as the wavemaker voltage. The shortest waves were sent first, with increasingly longer waves being sent out in sequence. Since the speed of an individual wave is proportional to the square root of its wavelength, a shorter wave will travel more slowly than a longer wave, and all the waves will meet at a prescribed distance from the wavemaker. These individual waves were chosen to combine approximately 200 feet from the wavemaker to create a breaking wave. The breaking wave was created using the voltage input shown with a blower speed of 1600 RPM. Figure 6 shows the typical shape of the resultant wave. Regular waves were generated by specifying blower speed (RPM) and frequency (Hz). Further details on the wavemaker can be found in (12).

Table 1. Test matrix.

Wave Height		Wave Length		Breaking	Face	Cube Angle	Plate Draft	Speed
(in)	(cm)	(ft)	(m)			(degrees)		(kts)
8,12,14	20.3,30.5,35.6	20	6.1	no	front	0,+45,-45	none,half,full	0
10	35.6	n/a	n/a	yes	front	0,+45,-45	none,half,full	0
8,12,14	20.3,30.5,35.6	20	6.1	no	top	0	half, full	0
10	35.6	n/a	n/a	yes	top	0	none,half,full	0
14	35.6	30	6.1	no	front	0	none	0.5,1,2
10	35.6	n/a	n/a	yes	front	0	none	0.5

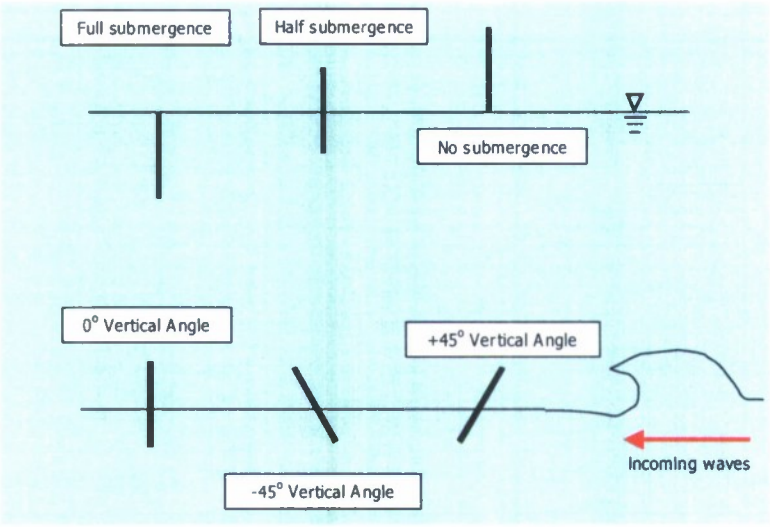

Figure 4. Instrumented plate submergence levels and angles.

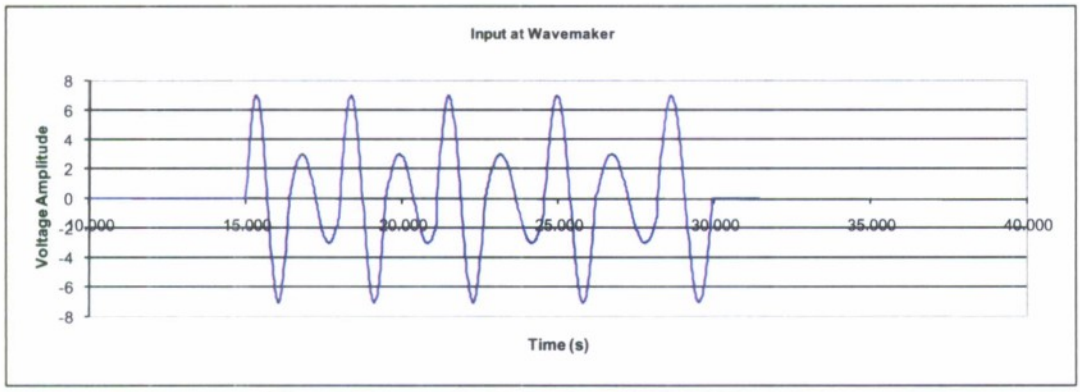

Figure 5: Wavemaker voltage input for breaking wave.

Table 2. Waves in the wavemaker input signal.

Wave	Amplitude (volts)	Period (s)	Start Time (s)
1	7	1.39	15.00
2	3	1.70	16.40
3	7	1.46	18.01
4	3	1.80	19.48
5	7	1.54	21.12
6	3	2.00	22.68
7	7	1.64	24.57
8	3	2.10	26.23
9	7	1.76	28.19

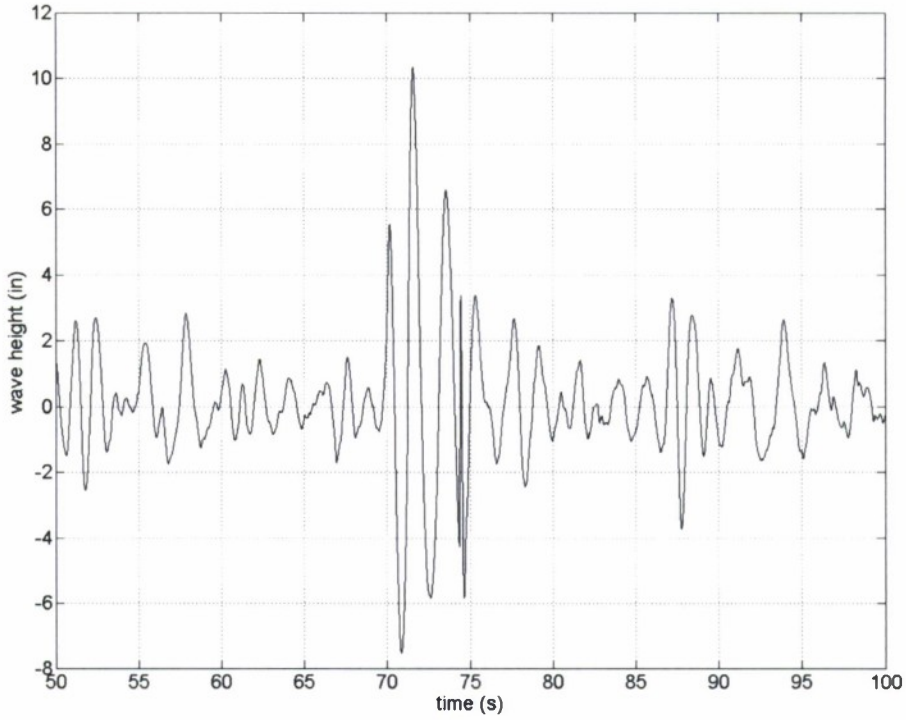

Figure 6: Wave measurement near plate.

Instrumentation

Slam panels

Nine slam panels were used on the instrumented faee of the eube, with the layout shown in Figure 7. The panels were made from rigid polyvinyl ehloride (PVC). A standard panel thickness of approximately 0.1 inches was used. Eaeh panel was instrumented with two strain gages wired into a Wheatstone bridge, whieh produeed an output voltage proportional to the differential bending of the panel. The panels were calibrated to a uniform pressure measurement over their area up to about 1 psi, which was performed by submerging the eube and relating the panel response to the pressure gage readings. The panels were set to eolleet pressure samples at a rate of 5 kHz.

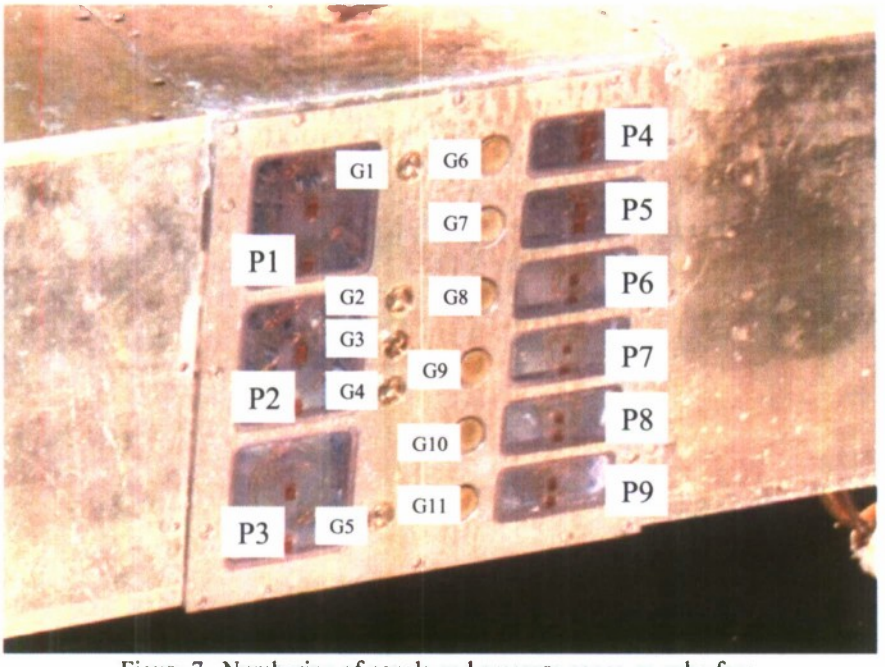

Figure 7. Numbering of panels and pressure gages on cube face.

Pressure gages

Eleven pressure gages were used on the instrumented face of the cube model. Six of the gages (G6-G11 in Figure 7) were the GE Novasensor NPI-19B-015AV, capable of measuring up to 15 pounds per square inch (psi). The GE Novasensor has a piezoresistive sensor chip housed in a fluid-filled cylindrical cavity which is isolated from the measured media by a stainless steel diaphragm and body, minimizing the temperature sensitivity of the gages. These gages have threaded ports which were fitted with a water-filled insert to prevent air from being trapped in the port. The other five pressure sensors were the GE Novasensor NPI-19A-015AV (shown as black circles on the left in Figure 3, G1-G5 in Figure 7). These are the same sensors as the other six, except that they have no port. All pressure gages were calibrated to 5 psi using air pressure, and gages were set to collect pressure samples at a rate of 5 kHz.

Dynamometer

Integrated force and moment measurements were made using a six degree-of-freedom dynamometer (NSWCCD serial number 2002-4). This dynamometer is comprised of two aluminum plates that have Kistler force gages between the plates at each of the four corners. Each gage measures force in three directions, and the total load is the sum of the four gages. Moments about all three axes can also be determined since the distance between the gages is known. The dynamometer was calibrated for a maximum load of 100 lbs. Details on the Kistler force gages can be found at http://www.kistler.com. The dynamometer was mounted between the cube and support structure, and was set to collect pressure samples at a rate of 5 kHz.

Senix Ultrasonic Sensors

The incoming waves were measured utilizing Senix ultrasonic distance sensors (Model TS-15S-IV), which are non-contact, ultrasonic instruments for measuring distances in air capable of measuring from 10 inches to 30 feet. Five sensors were utilized, with three in line with the incoming waves: one far forward of the impact region to measure the incoming wave, one just in front of the model to measure the impacting/reflected wave, and one in between. Another sensor was aligned with the one just in front of the model, but was offset from the plate to measure the wave height in absence of the model. The final sensor was located downstream of the cube to measure the wave height after impact. Figure 8 and Figure 9 show sketches of the experimental layout, which include the ultrasonic sensor locations labeled Sonic 2 through Sonic 5. Sonic 1 is located outside of the diagram. The differences between the two setups are the locations of the AWAC and the ADV, which switch positions about halfway through the test.

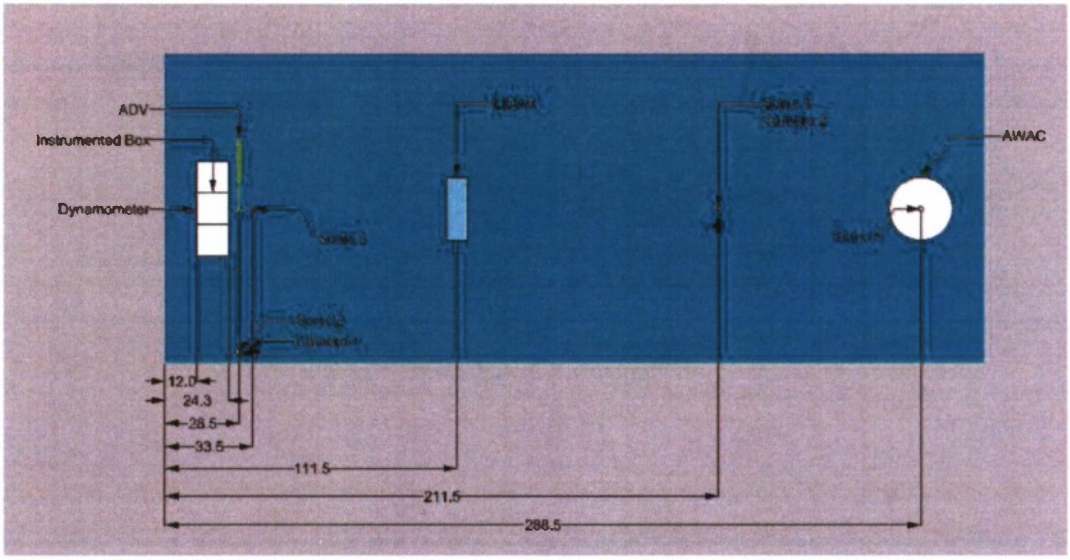

Figure 8. Plan view of experimental layout, setup 1. All measurements are in inches. Sonic 1 is located outside of the diagram.

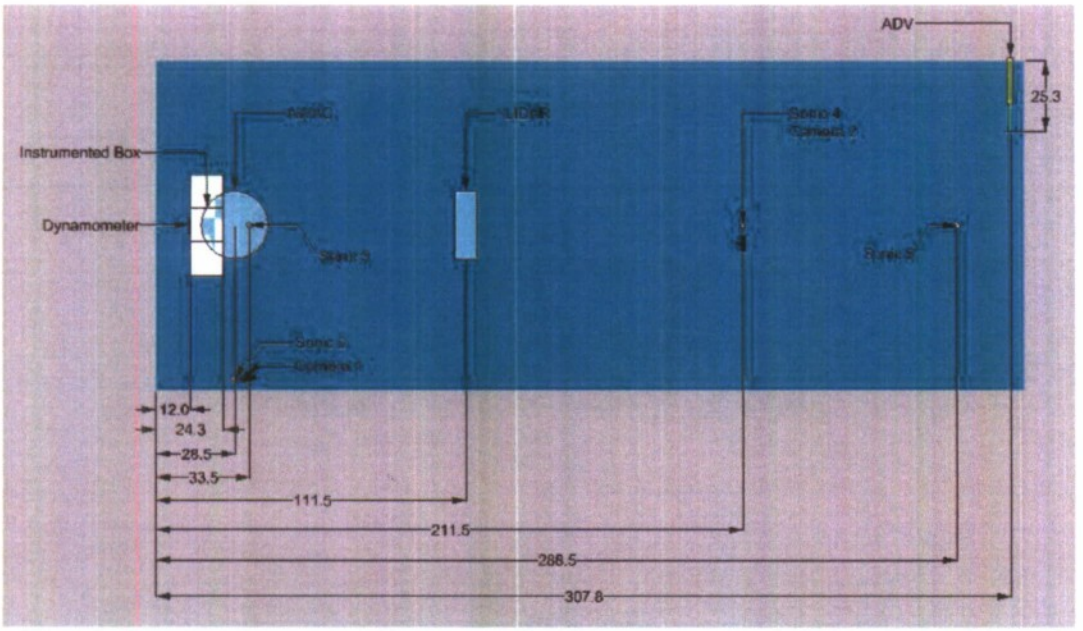

Figure 9. Plan view of experimental layout, setup 2. All measurements are in inches. Sonic 1 is located outside of the diagram.

LiDAR

Light Detection and Ranging, or LiDAR, is a remote sensing system used to collect topographic data. The LIDAR system used was equipped with a single Riegl pulsed laser mirror scanner (LMS-Q140-80i) and a four-sided mirror which spun to deflect the laser onto different angles and different positions along one line. This narrow laser beam then transmits pulses to a target and records the time it takes for the reflected pulse to echo back to the sensor receiver. The range accuracy of the LMS-Q140-80i unit is generally +/- 2cm, which typically scans in a +/- 40 degree sweep at a laser pulse repetition rate of 30 kHz. The LiDAR system was mounted above the carriage and measured the spatial wave field approaching the model. The LiDAR location is shown in the sketch in Figure 8.

Acoustic Wave and Current Profiler (AWAC)

The Nortek Acoustic Wave and Current Profiler (AWAC) is an acoustic Doppler current profiler (ADCP) with some added features (Figure 10). This instrument is capable of measuring current speed and direction in 1.6 ft thick layers from the bottom to the surface. An additional fourth acoustic beam is located in the center of the instrument head, which is used to track surface position acoustically. From this, the AWAC can measure wave height and direction for wave periods as short as 1.5s (in water depths of 5m or less). For a portion of the runs made, the AWAC was bottom-mounted directly under the cube model to measure velocities under the wave, as well as to track the position of the approaching wave. For the remaining runs made, the AWAC was used approximately 22 feet upstream of the cube to provide boundary condition velocities for

future computational work. The AWAC made surface position measurements at 4 Hz, and current measurements at 1 Hz. AWAC locations are shown in the sketch in Figure 8 and Figure 9.

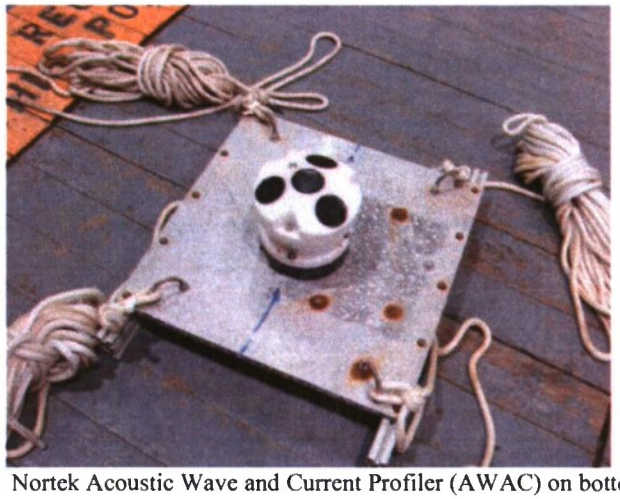

Figure 10. Nortek Acoustic Wave and Current Profiler (AWAC) on bottom mount

Acoustic Doppler Velocimeter (ADV)

The SonTek/YSI 10-MHz Acoustic Doppler Velocimeter (ADV) provides three dimensional velocity point measurements. The ADV is capable of sampling at a rate of up to 25 Hz, with a sampling volume of about 0.015 in^3, and an accuracy of 1% of the measured range. The ADV was mounted outboard of the cube model to measure velocity at the instrumented plate, and was also used approximately 22 feet upstream of the cube to provide boundary condition velocity for future computational work. It was traversed vertically to measure velocities at five different vertical positions during each run. Figure 11 shows the ADV on a vertical strut in front of the instrumented cube. The ADV locations are shown in the sketch in Figure 8.

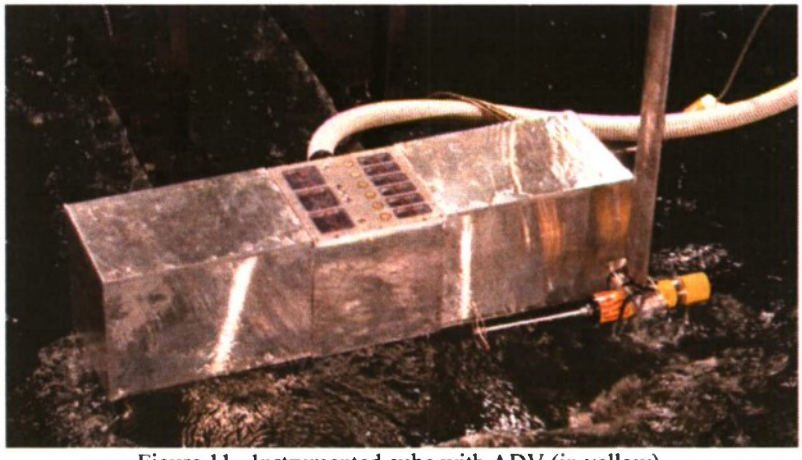

Figure 11. Instrumented cube with ADV (in yellow).

Standard and High Speed Video

Standard frame rate (30 frames per second) digital video eameras were used to reeord the visual appearanee of the free surface and wave impaets from a front and side view. High speed video was also used to eapture the visual wave impact on the instrumented face of the eube for a few selcet runs. The high speed video was reeorded at a rate of 500 frames per second, with a shutter speed of 1/500 frames per seeond. Figure 12 shows 3 frames from the high speed video capture for a breaking wave on the front face of the eube at a +45 degree angle.

Figure 12. Example of three frames from the high speed video for +45 degree angle, with breaking wave on front face.

Time Series

Figure 13 shows an example of the ADV velocity data for a wave height of approximately 8 inches and a wavelength of about 20 feet, with the test cube out of the water. Vx is the velocity in the direction of wave travel, and Vy is the vertical velocity. For these runs, the ADV is located about 9 inches below the calm water level. There is a dropout at around 272 seconds, which may have been caused by a lack of scatterers present in the water column at that time. The ADV appears to track the orbital wave velocities fairly well. All ADV data for this test is not included in this report, however, this information will be included in a future report.

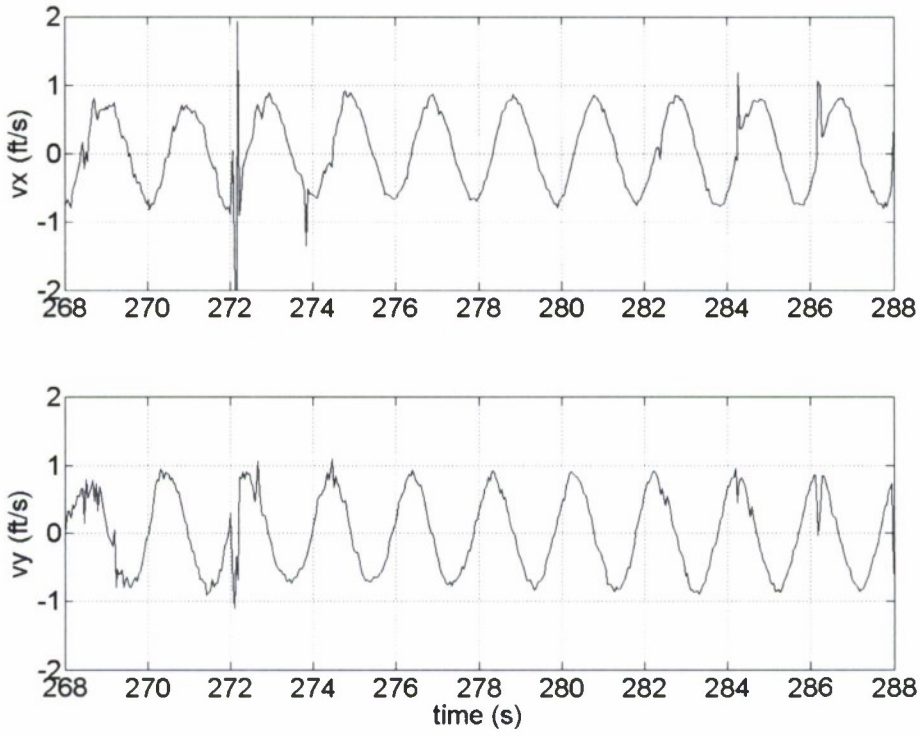

Figure 13. Example of ADV velocity data for wave height of approximately 8 inches and wavelength of 20 feet with the test cube out of the water. Vx is in direction of wave travel, and Vy is the vertical velocity.

Figure 14 shows an example of the AWAC surface tracking data for a wave height of approximately 8 inches and a wavelength of about 20 feet. The AWAC appears to capture the wave characteristics well. An example of the velocity measurements made by the AWAC are shown in Figure 15 at three different levels beneath the water surface, for a similar wave height. These velocities look different than the velocity measurements made by the ADV (Figure 13), which is to be expected since they are only collected at 1 Hz and are averaged over a 1.64 ft vertical bin. (The ADV records velocity data at a rate of 25 Hz and makes measurements over a 0.015 in^3 volume). All AWAC data for this test

are not included in this report, however, this information will be included in a future report.

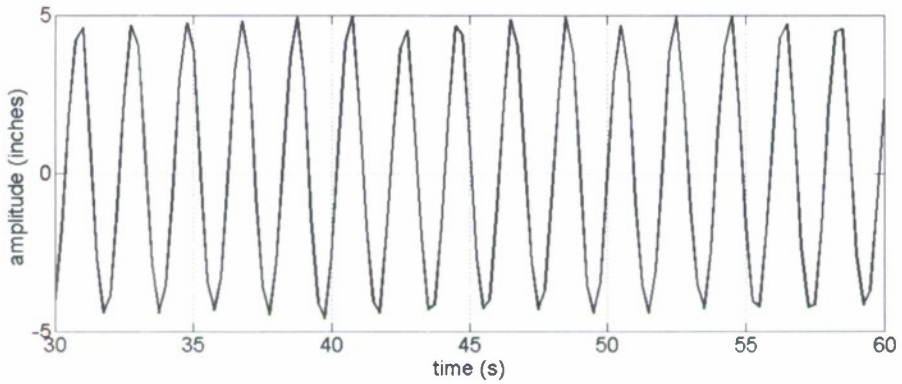

Figure 14. Example of surface tracking for AWAC for wave height of approximately 8 inches and wavelength of 20 feet with the test cube out of the water.

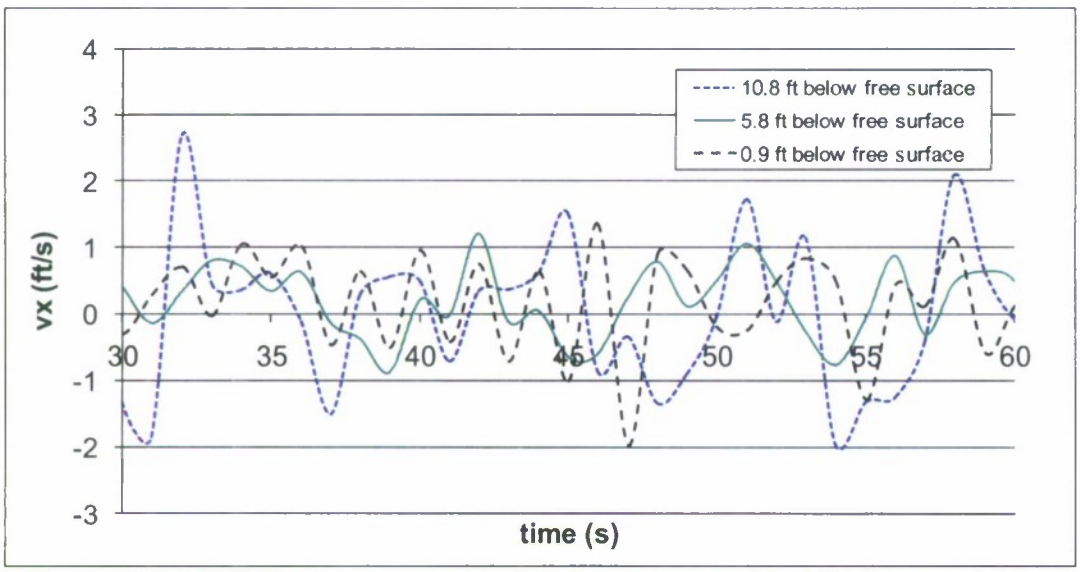

Figure 15. Example of velocity measurements in directions of wave travel for AWAC for wave height of approximately 8 inches and wavelength of 20 feet with the test cube out of the water.

Figure 16 shows the time series for the five ultrasonic sensors for an incoming wave approximately 12 inches in height, with a wavelength of 20 feet. The original time series is shown in black. The dropouts were removed and a highpass filter was applied to remove any drift in the sensor (most apparent in sensor number 2), which is shown with the red dashed line. Sensor number 2 reports a wave height that is much smaller than anticipated, though sensor numbers 1,3,4 and 5 seem to be showing similar wave heights to the desired results. It appears that sensor number 2 may have had some interference

from nearby struetures or from the other sensors and will not be used in the analysis. Another point of interest is the refleeted wave which is apparent in sensor number 3.

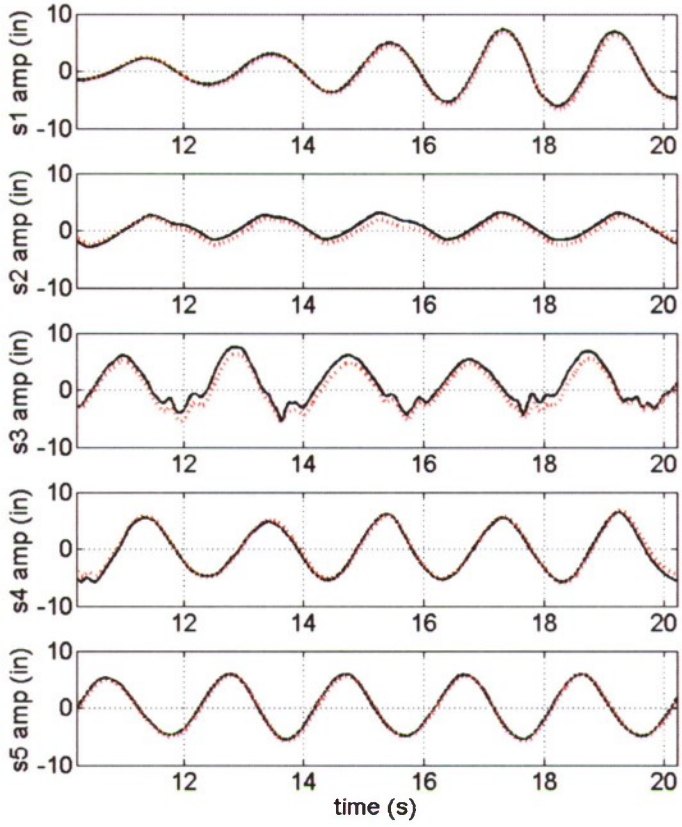

Figure 16. Example of data from ultrasonic sensor for wave height of approximately 12 inches and wavelength of 20 feet. The black line is the original signal and the red dashed line represents the filtered data with the dropouts removed.

Figure 17 and Figure 18 show pressure readings for panels 1 though 9 in psi. These plots also eorrespond to a wave approximately 12 ineheS in height, with a wavelength of 20 feet, for the instrumented panel on the front of the fully submerged eube with a zero degree angle. If there were no short duration impaets present, panel data were deeimated to 500 Hz to speed up analysis time. Additionally, if the panels were in a position out of the water and then hit with a wave (i.e. in a no submergence eondition or a top panel in a half submergenee eondition), a high pass median filter was applied to remove the temperature drift. The impact magnitudes for peaks above 0.05 psi for each wave eyele were then determined using a peak-finding program. This limit was ehosen beeause it appeared to be outside the inherent noise of the instrumentation. The first detected peak impaet was shown with a red asterisk, with the peak value noted next to the asterisk. The panels are zeroed before eaeh run, so for this fully submerged ease, the pressure reading ean be negative when the water level drops in a wave trough. In this way, the impaet from the ealm water position is measured. The pressure gages and

dynamometer are also zeroed before each run. Static measurements were made for each draft condition, and may be added back in for an absolute impact magnitude if desired.

Figure 19 and Figure 20 show the pressure readings for gages 1 through 11, for the same condition as previously described. Again, the first detected peak impact is shown with a red asterisk, with the peak value noted next to the asterisk. Pressure gage data are not decimated because of the short duration impacts that are present in most conditions. Figure 21 shows the force reading for the dynamometer for the same condition, and the first detected impact is again shown with a red asterisk.

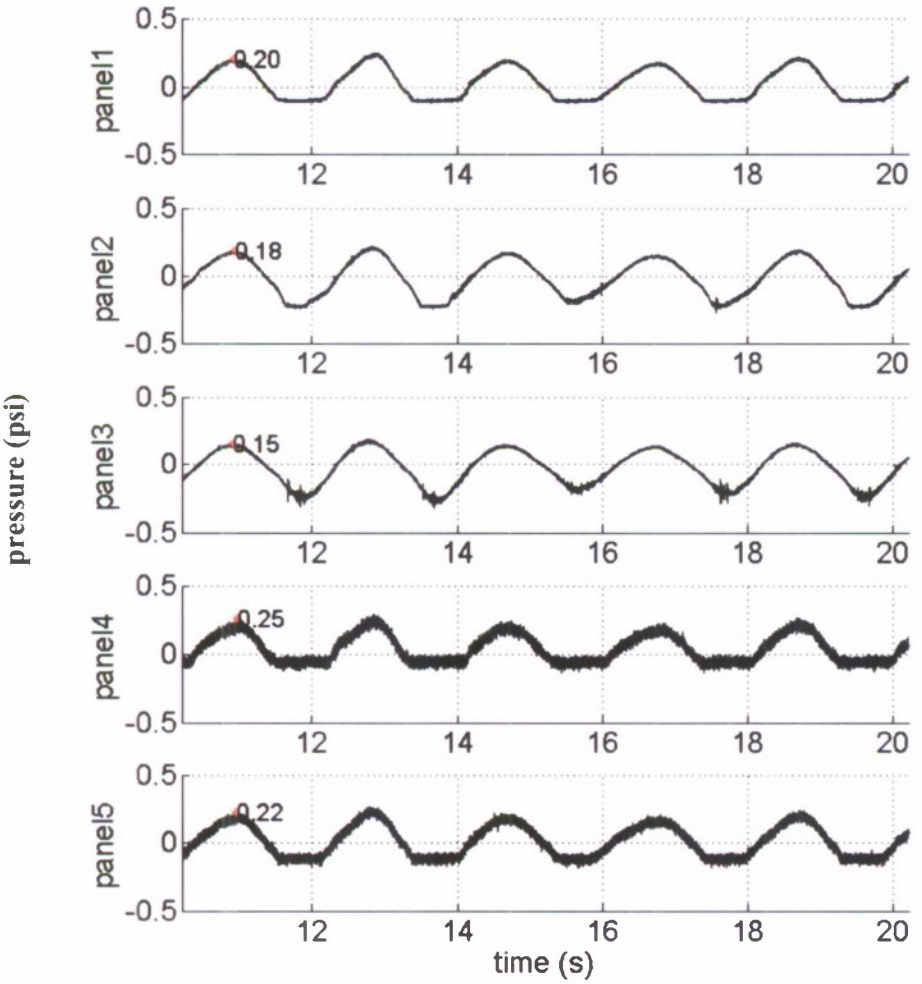

Figure 17. Example of data from panels 1 through 5 for wave height of approximately 12 inches and wavelength of 20 feet. All panel data is in psi, model scale, with a red asterisk noting the first peak location and text showing peak value.

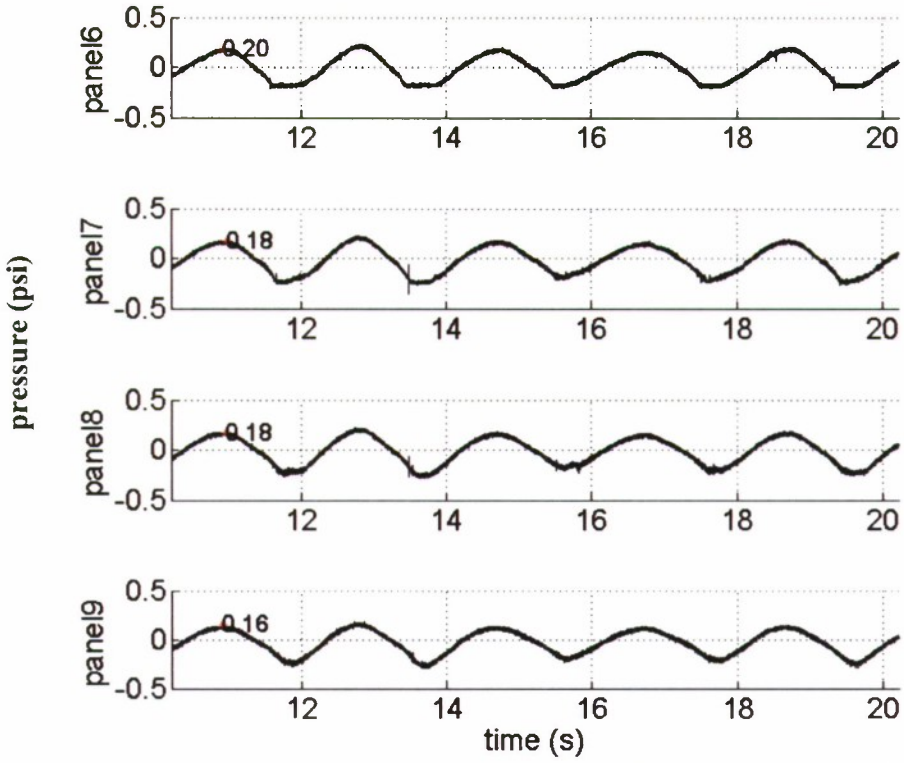

Figure 18. Example of data from panels 6 through 9 for wave height of approximately 12 inches and wavelength of 20 feet. All panel data is in psi, model scale, with a red asterisk noting the first peak location and text showing peak value.

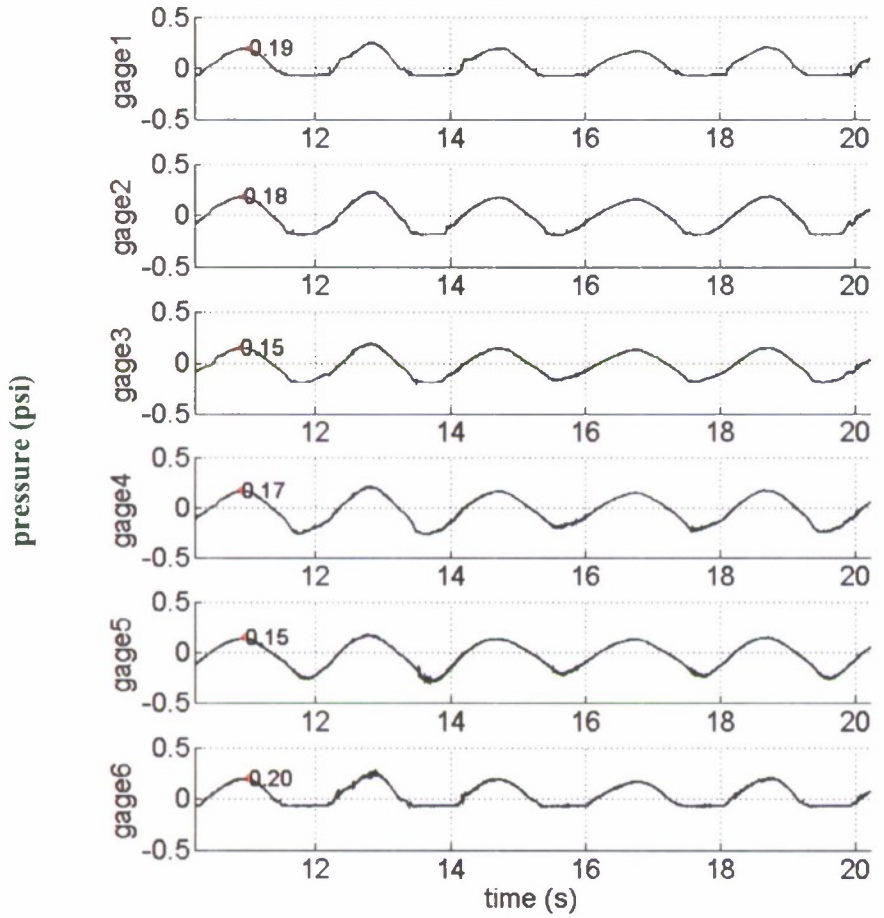

Figure 19. Example of data from pressure gages 1 through 6 for wave height of approximately 12 inches and wavelength of 20 feet. All pressure gage data is in psi, model scale, with a red asterisk noting the first peak location and text showing peak value.

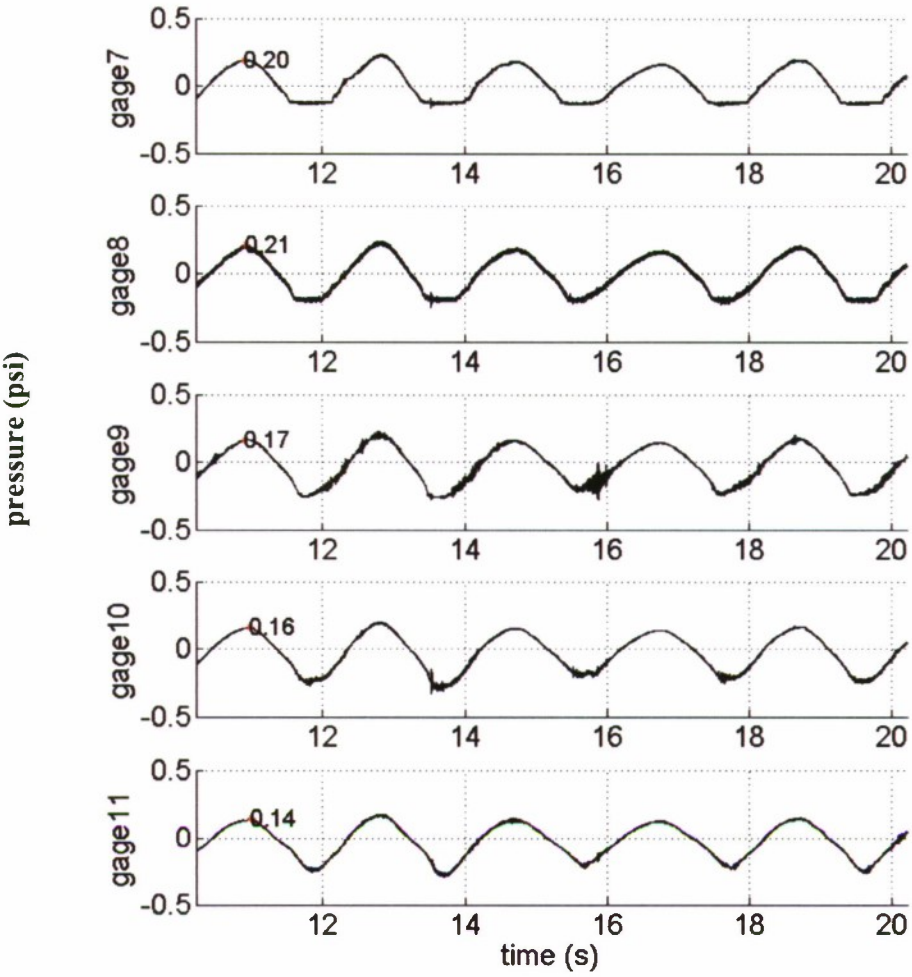

Figure 20. Example of data from pressure gages 1 through 6 for wave height of approximately 12 inches and wavelength of 20 feet. All pressure gage data is in psi, model scale, with a red asterisk noting the first peak location and text showing peak value.

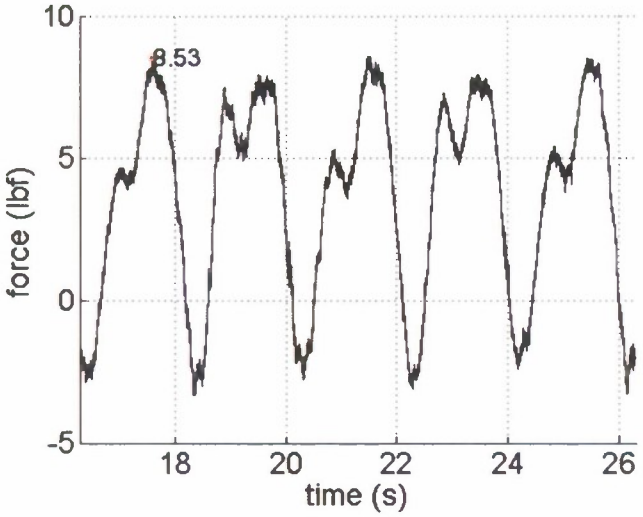

Figure 21. Example of wave force from dynamometer for wave height of approximately 12 inches and wavelength of 20 feet, with a red asterisk noting the first peak location and text showing peak value.

Wave Analysis

Data were collected for the non-breaking waves with the test cube out of the water in order to obtain wave measurements that would be independent by the cube. The average wave heights and wavelengths collected over 60 seconds are shown in Table 3, calculated using a zero crossing method and a spectral method. Ultrasonic sensor number 5 was used for this analysis because it appeared to collect the most reliable data, with the fewest number of dropouts. Average measured wave heights are close to those desired.

Figure 22 shows measurements made in the breaking wave condition using the ultrasonic sensor located just in front of the cube (though this run was made without the cube in place). The plot shows the variation in the wave height just before breaking, which is likely because the phases and heights of the waves that create this breaking wave change due to irregularities with the wavemaker. The average height before breaking is about 9.4 inches over 10 breaking waves; this value is similar to the average measurement of about 10 inches during the 2007 experiment (2).

Table 3. Summary of average wave measurements without cube.

Wave Height Desired	Spectral Analysis		Zero-crossing Method	
(in)	Height (in)	Length (ft)	Height (in)	Length (ft)
8	8.6	19.2	8.6	19.7
12	11.9	19.2	12.1	19.7
14	14.8	29.5	14.8	30.3

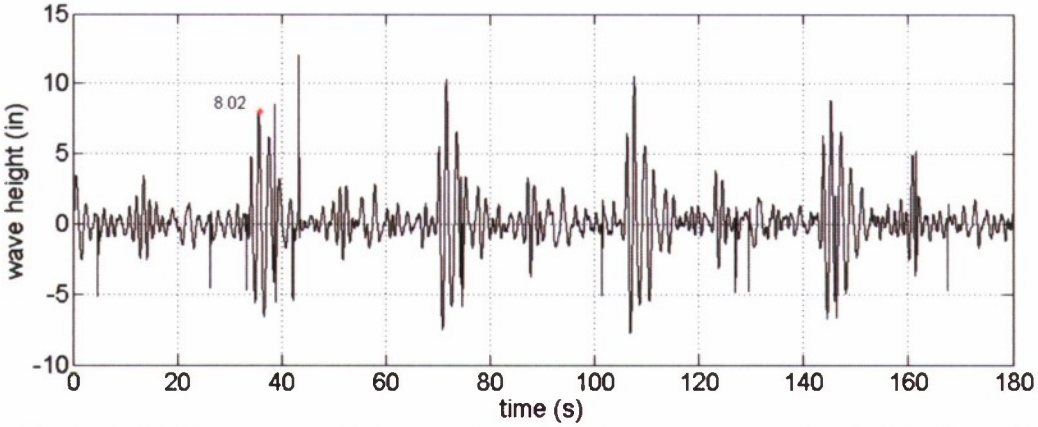

Figure 22. Breaking wave condition measurements from ultrasonic sensor number 3, with red asterisk noting peak location of first breaking wave and text showing peak value.

Impact Trends for Non-breaking Waves

Figure 23 shows the trends of the average impact pressures relative to the calm water condition on the nine slam panels from the non-breaking waves for all angles and submergences tested for the front face. The vertical bars on each data point represent the standard deviation of the averages. Overall, the pressures tend to increase with increased wave height. There is significantly more variation in the pressure measurements for the +45 degree angle, particularly for the largest waves. This is likely due to the presence of more short duration impact pressures in addition to the typical longer duration impacts, which may be caused by the +45 degree angle of the cube generating more wave breaking. These types of impacts are shown in the time series plot in Figure 24, which represents a front face, +45 degree angle, no submergence condition, with the detected peaks noted with red asterisks. Figure 25 shows an enlarged view of the full submergence, 0 degree angle case. This view shows that though there are differences in the panel measurements based on location, the general trends are the same.

Figure 26 shows the trends of the average impact pressures relative to the calm water condition on the pressure gages for the same conditions. These pressures tend to be higher than the panel readings, as expected, since they can respond much more quickly. Also, the localized pressures on the gages may be higher than the impact pressures averaged over the slam panel areas. Overall these pressures tend to increase with increased wave height similar to the panel pressures. Figure 27 shows an enlarged view of the full submergence, 0 degree angle case. This view shows that though there are differences in the gage measurements based on location, the general trends tend to be the same. Figure 28 shows the trends of the overall loads measured by the dynamometer. (Only the 0 degree angle loads are plotted; the +45 and –45 degree angles include buoyancy effects and may be misleading.) The trends are not as obvious for these measurements, and there is a significant amount of variation in the measurements, possibly due to thermal drift. It is interesting to note that the average load from the dynamometer over the entire face is about 0.3 psi (about 40 pounds divided by 144

square inches, the area of the face), which agrees fairly well with the average pressures measured by the slam panels.

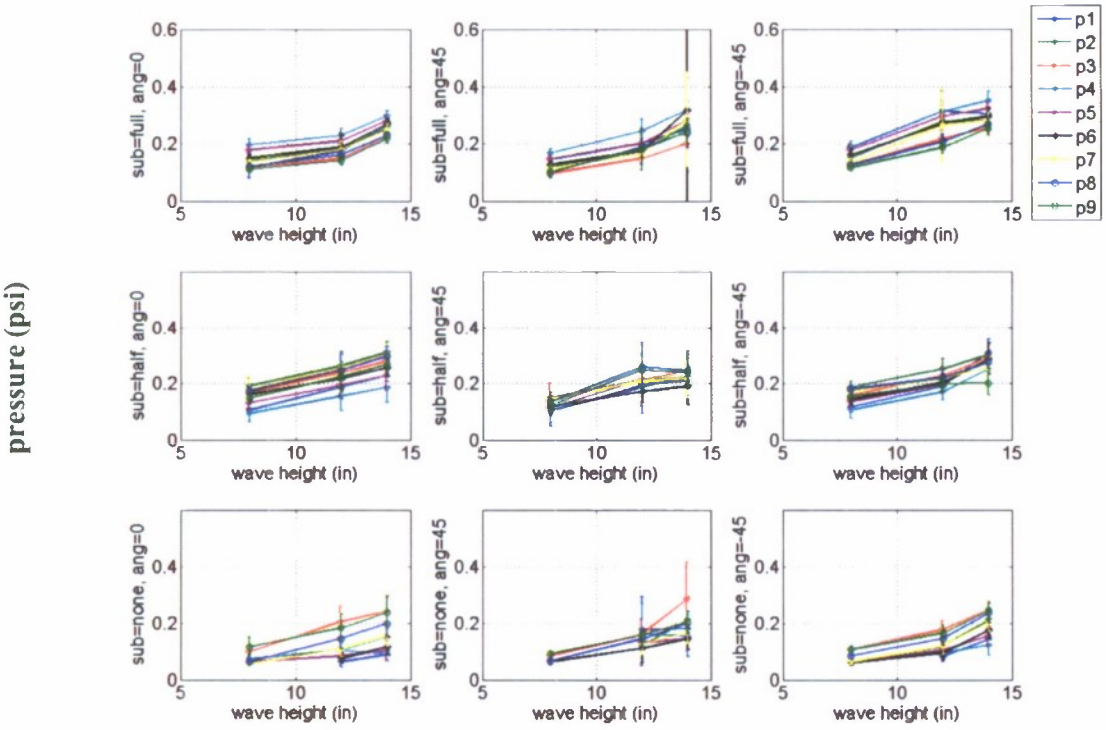

Figure 23. Trends of average impact pressures (psi) from panels on front face, for all non-breaking wave heights, submergences and angles tested.

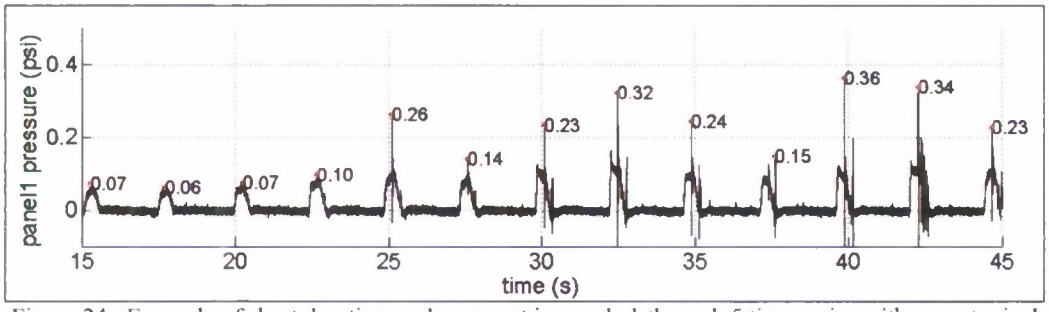

Figure 24. Example of short duration peaks present in panels 1 through 5 time series with more typical longer duration peaks. This plot represents a front face, 45 degree angle, no submergence condition. Detected peaks are noted with red asterisks.

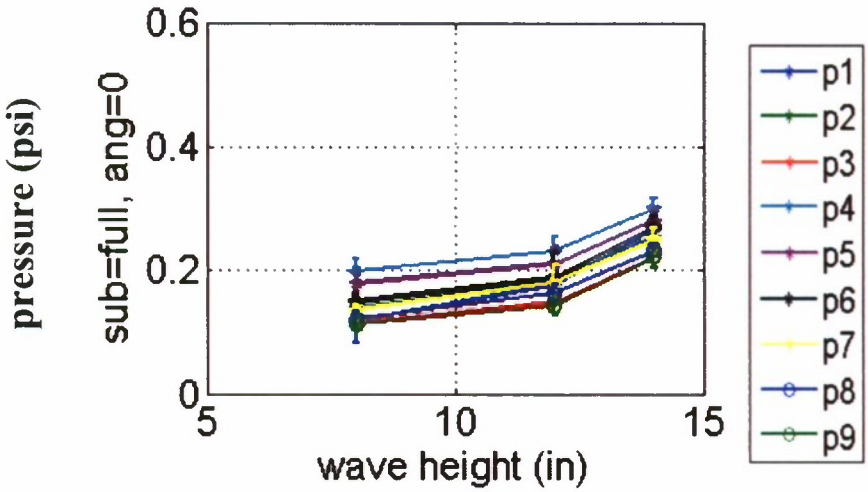

Figure 25. Enlarged view of trends of average impact pressures (psi) for panels on front face for full submergence, 0 degree angle case over all wave heights.

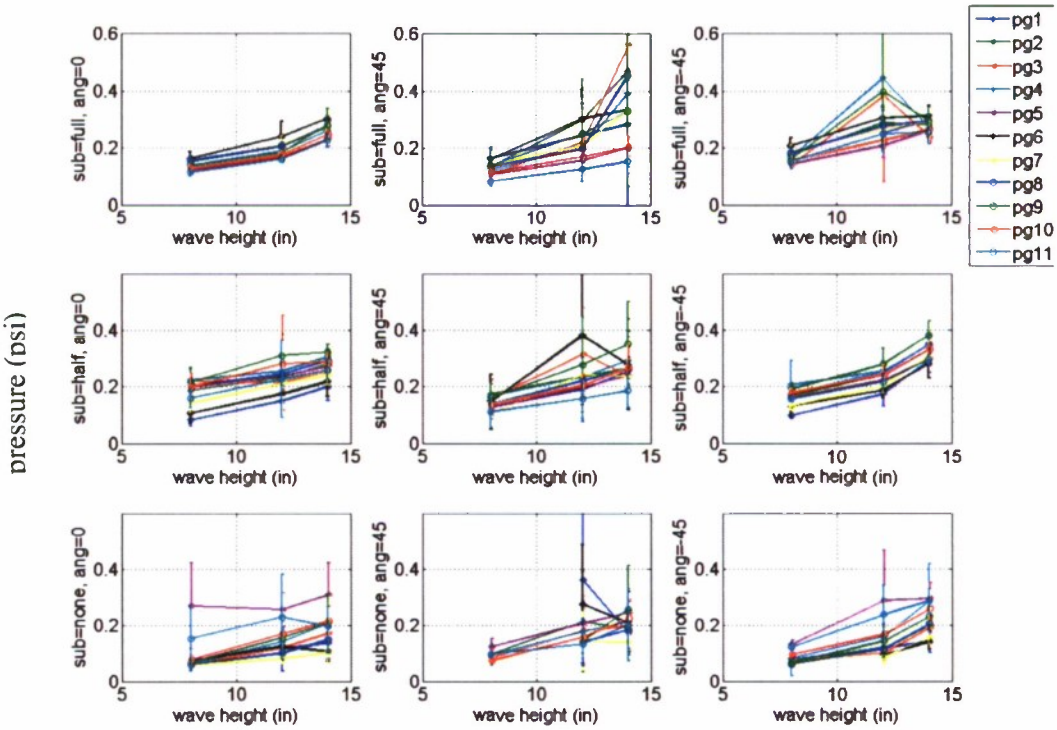

Figure 26. Trends of average impaet pressures (psi) from gages on front face for all non-breaking wave heights, submergences, and angles tested.

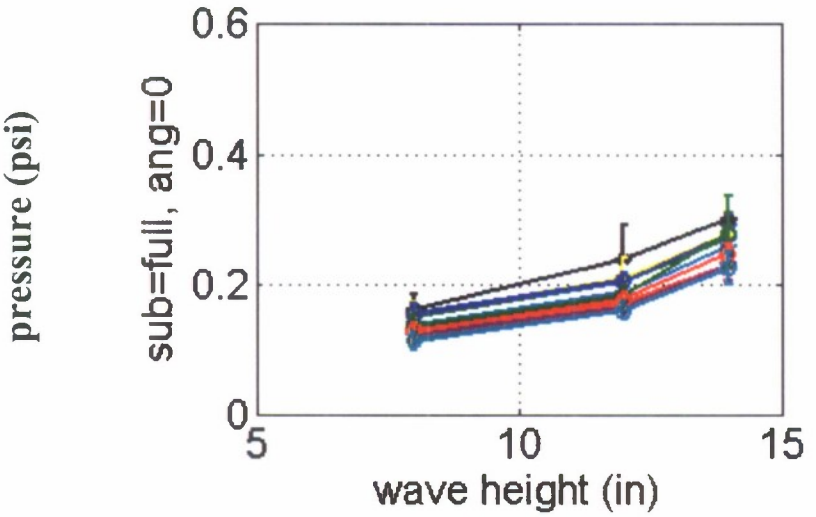

Figure 27. Enlarged view of trends of average impact pressures (psi) for gages on front face for full submergence, 0 degree angle case over all wave heights.

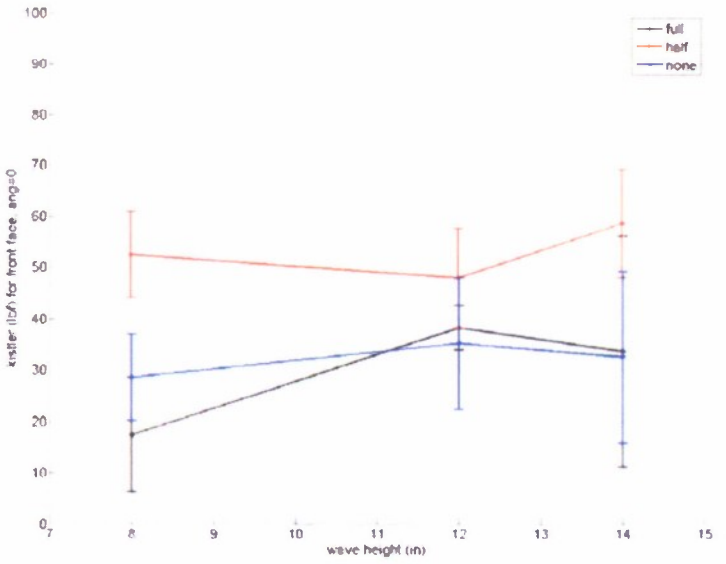

Figure 28. Trends of average impact pressures (psi) from the dynamometer on front face for all non-breaking wave heights and submergences for 0 degree angle, where a positive force is in the direction of wave travel.

Figure 29 shows the trends of the average impact pressures relative to the calm water condition on the panels on the top face from the non-breaking waves for all angles and submergences tested. Figure 30 shows the trends of the average impact pressures relative to the calm water condition on the pressure gages for the same conditions. Again, the vertical bars on each data point represent the standard deviation of the

averages. Pressures in this condition tend to be lower than the pressures measured on the front face. Also, there is significant variation in the measured pressures for the largest wave, possibly due to the wave breaking as it tops the cube.

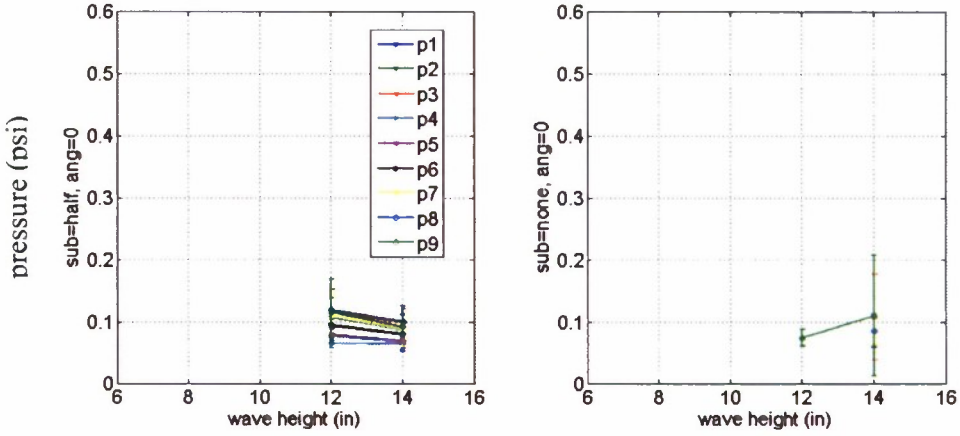

Figure 29. Trends of average impact pressures (psi) from panels for top face, for all non-breaking wave heights, submergences and angles tested.

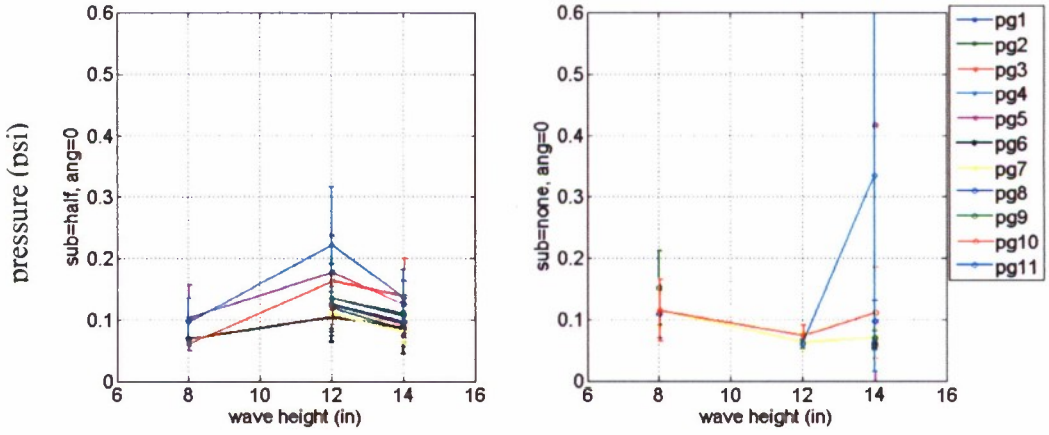

Figure 30. Trends of average impact pressures (psi) from pressure gages for top face, for all non-breaking wave heights, submergences and angles tested.

Impact Trends for Breaking Waves

Figure 31 shows the trends of the average impact forces relative to the calm water condition on the front face slam panels from the breaking waves, for all submergences and angles tested. Figure 32 shows similar plots for the pressure gages for the same conditions. Overall, the impact forces are greater in magnitude for the breaking waves than for the non-breaking waves. The condition that yields the greatest pressures is the

+45 degree angle position, which has the cube angled toward the incoming waves, similar to the trends in non-breaking condition. Additionally, for this condition, the upper panels (panels 1,4 and 5) experience larger magnitude impacts than the lower panels, possibly because they get hit with the fastest part of the wave (the crest). The 0 and -45 degree angle yield pressures in similar ranges, and are both lower in magnitude than the +45 degree angle condition. The pressure gage results show similar trends, but with mostly greater magnitudes, again because they can respond much more quickly wave impacts. Also, the localized pressures on the gages may be higher than the impact pressures averaged over the slam panel areas. Figure 33 shows the trend of the overall loads measured by the dynamometer. (Only the 0 degree angle loads are plotted; the +45 and –45 degree angles include buoyancy effects and may be misleading.) The trends are not as obvious for these measurements, and there is a significant amount of variation in the measurements, possibly due to thermal drift. Overall, these loads are larger in magnitude than measured for the non-breaking waves.

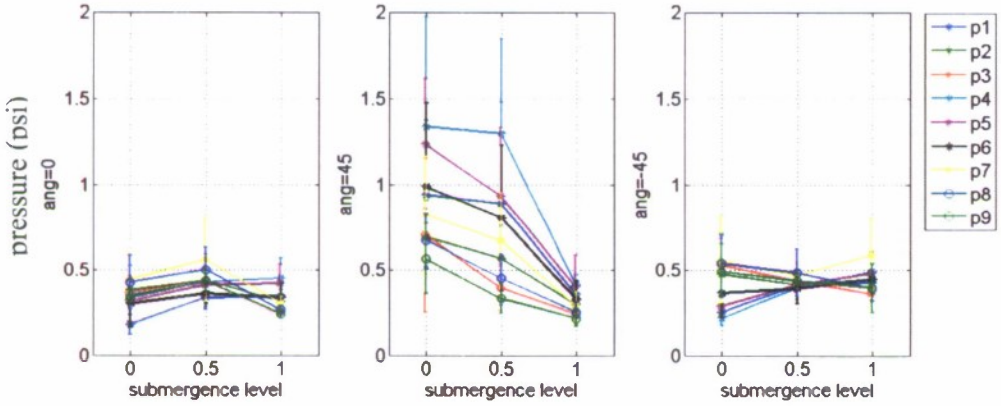

Figure 31. Trends of average impact pressures (psi) from panels for front face, for breaking waves, all submergences and angles tested.

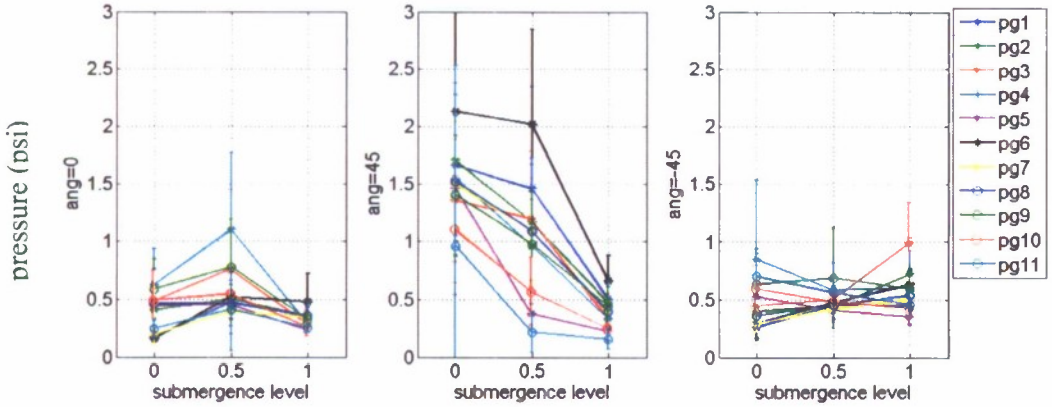

Figure 32. Trends of average impact pressures (psi) from pressure gages for front face, for breaking waves, all submergences and angles tested.

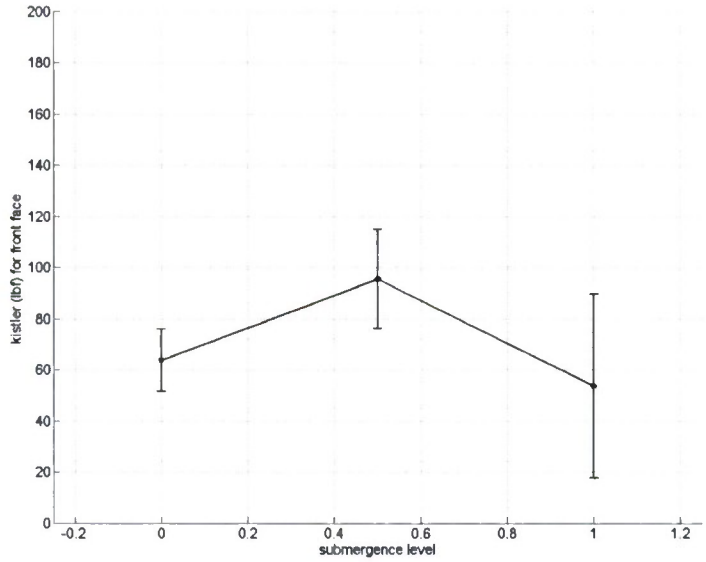

Figure 33. Trends of average impact pressures (psi) from the dynamometer for front face, for breaking waves, for 0 degree angle and all submergences tested.

Figure 34 shows the average breaking wave impact pressure trends relative to the calm water condition for the top face panels for all angles and submergences tested. Figure 35 shows the trends of the average impact pressures relative to the calm water condition on the pressure gages for the same conditions. Again, the vertical bars on each data point represent the standard deviation of the averages. Pressures in this condition tend to be larger than the pressures measured from the non-breaking waves on the top face.

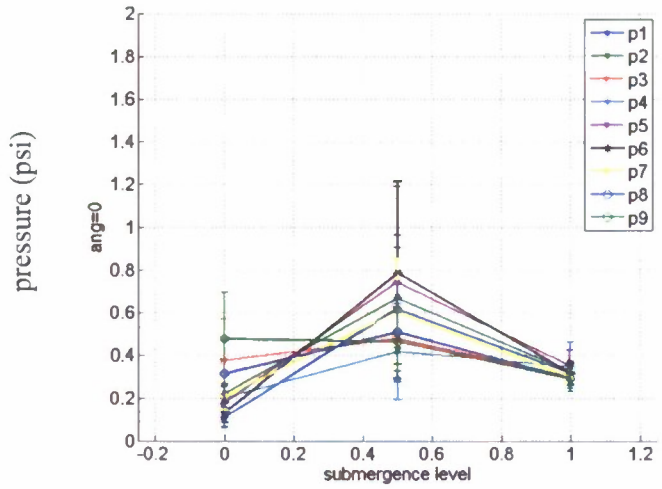

Figure 34. Trends of average impact pressures (psi) from panels for top face, for breaking waves, all submergences and angles tested.

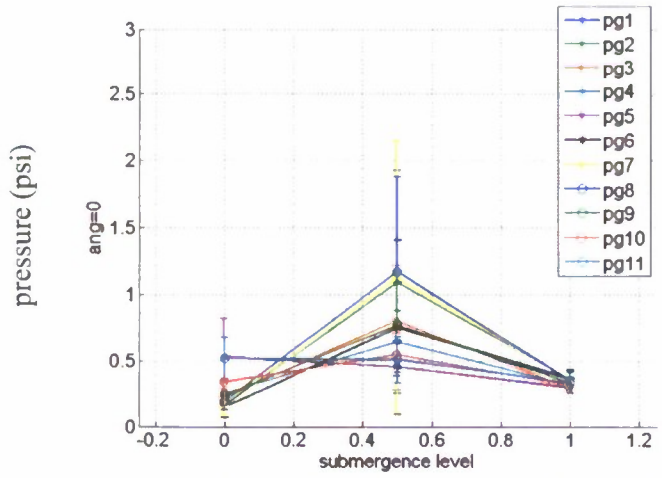

Figure 35. Trends of average impact pressures (psi) from pressure gages for top face, for breaking waves, all submergences and angles tested.

Impact Trends with Speed

The cube was tested at speeds of 0.5, 1 and 2 knots for the 0 degree angle, for the no submergence condition in wave heights of 14 inches, in addition to the 0 speed runs discussed previously. Results from the slam panels, pressure gages and dynamometer are shown in Figure 36, Figure 37, and Figure 38, respectively. The average impact forces on the lower panels (8 and 9) increase with speed. On average, the impact forces increase with speed for the upper panels as well, though there is a dip in the average at 1 knot. There is also a large amount of variation in the pressures at 1 knot. Similar trends can be

seen on the pressure gages (with mueh more variability) as well as with the dynamometer.

Table 4 lists the impaet forces measured on the panels for the breaking wave at zero speed, and at 0.5 knots. In general, the loads inerease in magnitude from 0 speed to with speed, as was seen with the non-breaking waves.

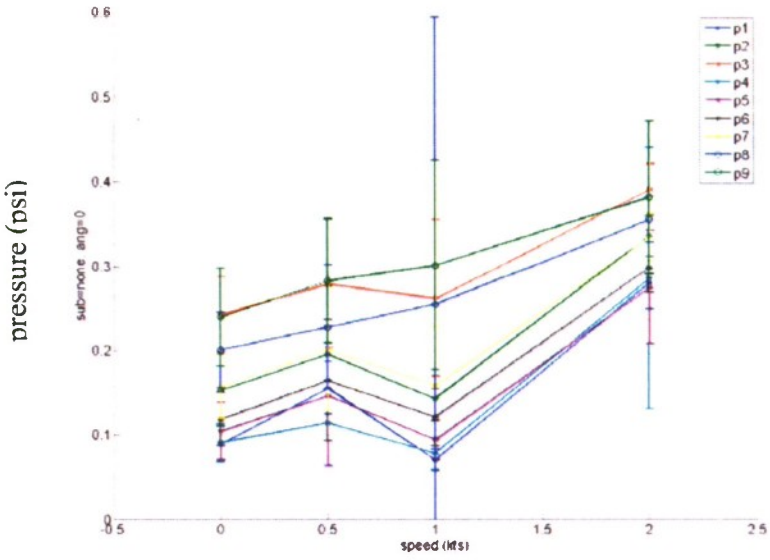

Figure 36. Trends of average impact pressures (psi) from panels for front face, for non-breaking waves, for 0 degree angle and no submcrgence, across a range of speeds.

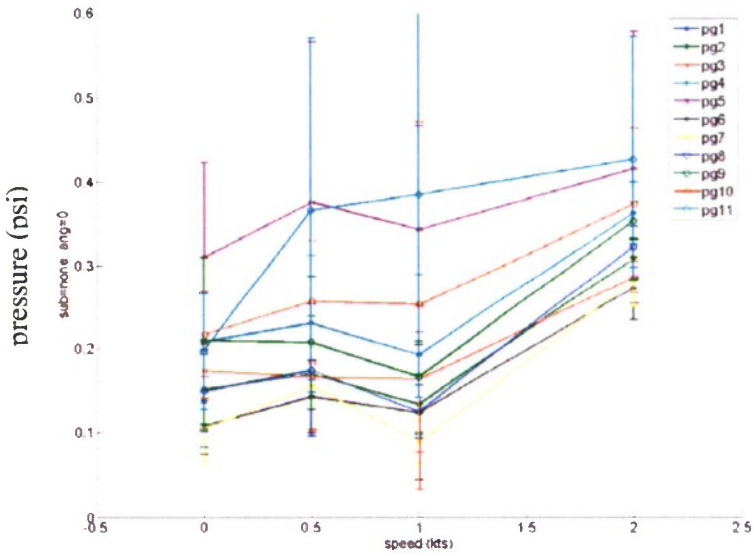

Figure 37. Trends of average impact pressures (psi) from gages for front face, for non-breaking waves, for 0 degree angle and no submergence, across a range of speeds.

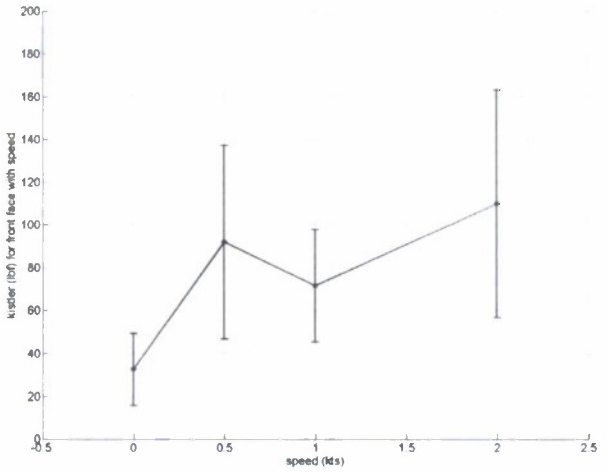

Figure 38. Trends of average impact pressures (psi) from the dynamometer for front face, for non-breaking waves, for 0 degree angle and no submergence, across a range of speeds.

Table 4. Summary of breaking wave impact loads on the front face at 0 speed and at 0.5 knots for 0 degree angle and no submergence.

Panel Number	Breaking pressure at 0 speed (psi, average)	Breaking pressure at 0.5 knots (psi)
1	0.18	0.57
2	0.38	0.50
3	0.36	0.46
4	0.35	0.55
5	0.31	0.57
6	0.30	0.50
7	0.44	0.47
8	0.42	0.43
9	0.33	0.53
dynamometer	70.7 lbf	166 lbf

CONCLUSIONS

This experiment has provided a data set of the distribution of impact pressures from incident non-breaking and breaking waves on one face of a cube, with various cube face orientations, face angles, and submergence depths. A number of observations can be made from the results of this experiment, including:

- There is more variation in average impact pressures for the +45 degree angle than for the 0 or –45 degree angle likely because there are more short duration, higher magnitude impacts in addition to the more typical longer duration impacts. This greater number of

higher magnitude impacts is probably due to increased wave breaking under the +45 degree angle orientation.

- Pressure gage readings tend to be higher than the panel readings, as expected, since they can respond much more quickly to the short duration, localized impacts present and because they cover a smaller area than the slam panels.
- Pressures from non-breaking waves on the top face tend to be lower than the pressures on the front face.
- Overall, average impact pressures from the breaking waves are greater in magnitude than the impact pressures from the non-breaking waves.
- Overall, average impact pressures tend to increase with increased speed, though there was a dip in pressure at an intermediate speed for some panel locations, and only a small range of low speeds was tested.

This data set has provided more insight to the trends and characteristics of wave impact loads. A more detailed analysis of this data would certainly be useful, including:

- A detailed comparison of the impact loads on the larger panels versus the smaller panels in the same locations.
- Investigation of trends of integrated pressures over impact time (as opposed to peak magnitude) with wave characteristics.
- Investigation of wave slope effects on the impact force.
- Investigation of causes of short duration impact loads versus the more typical, longer duration loads.
- Development of wave load prediction using wave height, face orientation, face angle, and submergence depth in an empirical equation or neural network.
- Analysis of relationship between impact pressures and velocities measured by the ADV and AWAC.

Additionally, more experimental work would be useful in advancing the understanding of wave impact load trends. Further work should be done with the existing model, possibly in a facility with more controlled wave conditions so that the wave phase could be more accurately prescribed, or the test could be expanded with more wave heights, wavelengths and forward speeds. This would provide the ability to reconstruct an environment that causes the short duration, high magnitude impacts, which would provide insight to the environmental parameters that cause these severe impacts. Another possible sequence of experiments would be to measure the distribution of wave impact loads on other simple geometries, possibly a cylinder or sphere, while also varying wave characteristics.

REFERENCES

1. Chan, E.-S. and W.K. Melville (1984). "Breaking wave forces on surface-piercing structures." Oceans '84, Washington, D.C., pp. 565-570.

2. Chan, E.-S. and W.K. Melville (1987). "Plunging wave forces on surface-piercing structures." In: Proc. 6th Intl. Offshore Mech. and Arctic Eng. Symposium, ASME, Houston, TX, 2: 61-72.

3. Chan, E.S. and W.K. Melville (1988). "Deep-water plunging wave pressures on a vertical plane wall." Proc. R. Soc. Lond, A417: 95-131.

4. Chan, E.-S. and W.K. Melville (1989). "Plunging wave forces on surface-piercing structures." Trans. ASME, J. of Offshore Mechanics and Arctic Engineering, 111: 92-100.

5. Zhou, D., E.-S. Chan and W.K. Melville. (1991). "Wave-impact pressures on vertical cylinders." Appl. Ocean Res., 13: 220-234.

6. Bullock, G. and C. Obhrai (2001). "Wave Impact Loads at Large and Full Scale." Coastal Zone Network. Available at: http://cozone.org.uk/overtop/15-GB.pdf

7. Pence, A. M., T. C. Fu, M. Jiang, and Y. S. Hong. *Investigation of Wave Impact Load Guidelines for Ship Appendages*. International Offshore and Polar Engineering Conference (ISOPE-2006), June 2006, San Francisco, CA, USA.

8. Hess, D. , W. Faller, R. Roddy, A. Pence, and T. Fu. *Feedforward Neural Networks Applied to Problems in Ocean Engineering*. Proceedings of OMAE 2006, 25th International Conference on Offshore Mechanics and Arctic Engineering, June 4-9, 2006, Hamburg, Germany.

9. Fullerton, A.M., Fu, T.C., and D. Hess. *Feedforward Neural Networks Applied to Problems in Ocean Engineering*. Proceedings of OMAE 2007, 26th International Conference on Offshore Mechanics and Arctic Engineering, June 10-15, 2007, San Diego, CA, USA.

10. Fu, T.C., Fullerton, A.M., Brewton, S., Brucker, K.A., and D. Dommermuth. *An Experimental and Computational Study of Breaking Wave Impact Forces*. 27th Symposium on Naval Hydrodynamics, October 5-10, 2008, Seoul, Korea.

11. Schoenherr, K. E. & Brownell, W. F. "The High-Speed Basin and Instrumentation at the David Taylor Model Basin," DTMB Report 1660, January 1963.

12. Stahl, Ralph. *NSWCCD Wavemakers and Notes on Wavemaking*. CRDKNSWC/HD-0369-12, Hydromechanics Department Report, June 1998.

This page intentionally left blank.

DISTRIBUTION

Copies		Name
1	PSU/ARL	Paterson
NAVSEA		
1	DTIC	
2	05Z	King, Lee (pdf only)
ONR		
1	331	Joslin
Division Distribution		
1	3452	Library (pdf only)
1	5060	Walden
3	5700	Brewton, Gorski, Jiang (pdf only)
5	5600	Ammeen, Drazen, Hess, Merrill, Wade (pdf only)
4	5800	Fu, Fullerton (pdf only), office files (2)
2	653	Hay, Lewis, Powers (pdf only)
1	65	Rasmussen (pdf only)